



**Evidence for correlation effects in noncentrosymmetric type-II Weyl semimetals**M. Corasaniti <sup>1,\*</sup>, R. Yang <sup>1,\*</sup>, Z. Hu,<sup>2,3</sup> M. Abeykoon,<sup>4</sup> C. Petrovic,<sup>2,3</sup> and L. Degiorgi <sup>1,†</sup><sup>1</sup>Laboratorium für Festkörperphysik, ETH - Zürich, 8093 Zürich, Switzerland<sup>2</sup>Condensed Matter Physics and Materials Science Department, Brookhaven National Laboratory, Upton, New York 11973, USA<sup>3</sup>Department of Materials Science and Chemical Engineering, Stony Brook University, Stony Brook, New York 11790, USA<sup>4</sup>National Synchrotron Light Source II, Brookhaven National Laboratory, Upton, New York 11973, USA

(Received 9 April 2021; revised 4 August 2021; accepted 8 September 2021; published 20 September 2021)

Topological fermions have mainly been addressed in the limit of weakly correlated systems, while the realization of Kondo-like physics arising from Dirac-Weyl fermions and implying strong correlations is rare. The noncentrosymmetric Weyl fermion  $R\text{AlGe}$  compounds (with  $R = \text{La}$  and  $\text{Ce}$ ) provide a promising playground for revealing the impact of electronic correlations driven by  $f$ -electron states on Weyl fermions. Here, we tackle their charge dynamics as a function of temperature. Besides spotting typical optical signatures of a type-II Weyl semimetal in both materials, we discover that electronic correlations at low temperatures renormalize the nontrivial bands hosting the Weyl nodes and lead to a reduction of the Fermi velocity as well as an enhancement of the charge carriers effective mass in  $\text{CeAlGe}$  with respect to  $\text{LaAlGe}$ , both being a fingerprint of a so-called Weyl-Kondo system.

DOI: [10.1103/PhysRevB.104.L121112](https://doi.org/10.1103/PhysRevB.104.L121112)

The interplay of topology with electronic correlations is acquiring increasing interest in the ongoing solid-state physics research and leads to concepts of paramount importance for the understanding of novel functionalities in quantum materials [1–3]. Charge, spin, and orbital degrees of freedom of electrons in solids are intimately related to and shaped by the topological nature of the host material. For instance, a topological state of relevance in condensed matter derives from the split of the doubly degenerate, massless Dirac states into a pair of Weyl nodes, as a consequence of broken time-reversal or space-inversion symmetry [4,5]. On the other hand, electronic correlations are a basic asset for materials featuring a large variety of astonishing properties [6]. The link between topology and many-body ground states has been explored only recently, with proposals advancing topological Weyl superconductors [7] and charge-density-wave states in Weyl semimetals [8–10], as well as Weyl-Mott insulators [11].

Another possible consequence of electronic correlations is exemplary epitomized by the Kondo materials, for which the coupling between  $f$ -electrons and conduction-band states notably leads to strong renormalization of the electronic bands in the vicinity of the Fermi energy ( $E_F$ ), then possessing  $f$ -character and displaying the formation of heavy electrons at low temperatures ( $T$ ) [12]. Several topological phases are emerging, when the single-particle band structure is modified by Kondo-like electron-electron correlations, within concepts ranging from hybridization-driven heavy Weyl-Kondo

semimetals [13,14] to Kondo effects of magnetic impurities in Dirac and Weyl systems [15,16].

While  $\text{CeRu}_4\text{Sn}_6$  was proposed as a promising heavy Weyl fermion candidate [17],  $\text{Ce}_3\text{Bi}_4\text{Pd}_3$  [13,18,19] and  $\text{YbPtBi}$  [20] are, to date, among the rare experimental realizations of a Weyl-Kondo compound. This motivates the investigation of condensed matter systems providing the tunability of the Kondo coupling in an environment of Weyl states, upon switching-on the presence of  $f$ -electrons.

In this respect, the family of the noncentrosymmetric  $R\text{AlGe}$  ( $R = \text{rare earth}$ ) compounds [21] is a suitable arena to advance our knowledge. First of all,  $R\text{AlGe}$  span all varieties of Weyl semimetals depending on the choice of  $R$ ; namely, the standard type I with point-like Fermi surface and the initially overlooked type II arising from the tilting of the Weyl cones with the Fermi level along the line boundaries of electron and hole pockets [21–23]. Second,  $\text{LaAlGe}$  ( $4f^0$  orbitals) is non-magnetic, while first-principles calculations prefigure  $\text{CeAlGe}$  (with  $\text{Ce } 4f^1$ ) and  $\text{PrAlGe}$  (with  $\text{Pr } 4f^2$ ) to order ferromagnetically [21]. Even though the magnetism in  $\text{CeAlGe}$  is matter of debate [24–28], it turns out that the prediction of Weyl nodes in  $R\text{AlGe}$  as well as their band structure at low energies seem to be robust enough and less dependent on the details of the magnetism [21]. We note in passing that the presence of both time-reversal and space-inversion broken symmetry should favor spin current without concomitant charge current [29], an aspect of both fundamental and technical interest. Third, it has been postulated [13,14,20] that the Kondo coupling between  $f$ -electrons and bands hosting the Weyl nodes close to  $E_F$  could lead to a greatly reduced Fermi velocity ( $v_F$ ) and to the enhancement of the itinerant quasiparticles effective mass ( $m^*/m_e$ ) compared to the bare band values at low  $T$ .

The signatures of Weyl fermions as well as  $m^*/m_e$  and  $v_F$  are accessible from the excitation spectrum. In this letter,

\*These authors contributed equally to this work.

†degorgi@solid.phys.ethz.ch; Correspondence and requests for materials should be addressed to L. Degiorgi, Laboratorium für Festkörperphysik, ETH - Zürich, 8093 Zurich, Switzerland.

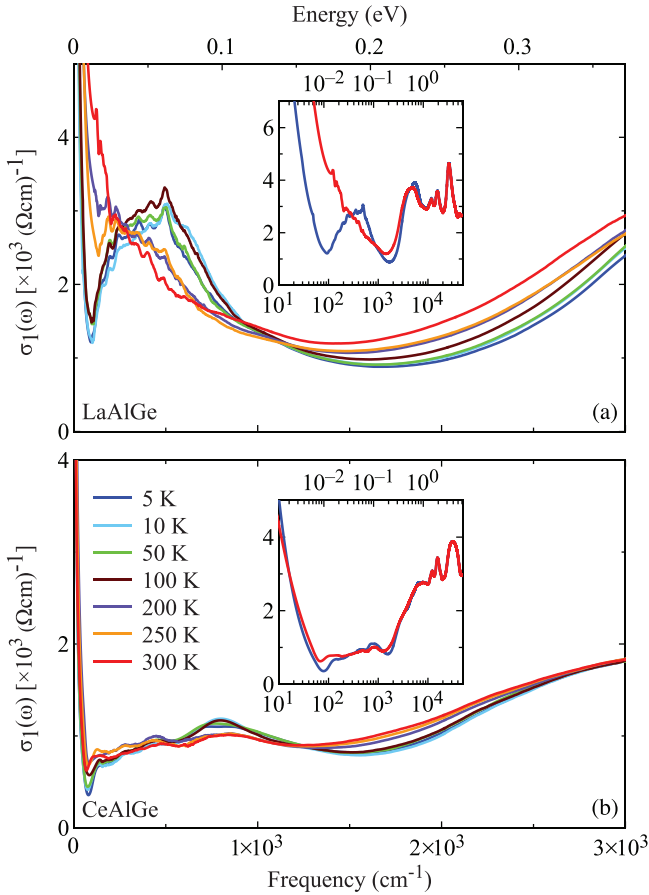


FIG. 1.  $T$  dependence of the real part  $\sigma_1(\omega)$  of the optical conductivity of (a) LaAlGe and (b) CeAlGe from the far-infrared up to the midinfrared frequency range ( $1 \text{ eV} = 8.06548 \times 10^3 \text{ cm}^{-1}$ ). The insets show  $\sigma_1(\omega)$  in the entire measured energy interval at 300 and 5 K (please note the logarithmic energy scale).

we exploit the  $T$  dependence of the real part [ $\sigma_1(\omega)$ ] of the optical conductivity of LaAlGe and CeAlGe, obtained over a very broad energy interval from the far-infrared (FIR) up to the ultra-violet (UV) spectral range [30]. While a variety of representative Dirac and Weyl semimetals were recently addressed from the perspective of their optical response (see Ref. [31] for a recent review), our results display the characteristic interband feature in  $\sigma_1(\omega)$  of the less scrutinized type-II Weyl semimetals as well as a depleted  $v_F$  and a remarkably enhanced quasiparticles  $m^*/m_e$  at low  $T$  in CeAlGe than in LaAlGe. Our inferences are thus of guiding relevance when establishing Kondo-like physics in these noncentrosymmetric (type-II) Weyl semimetals.

We start off with a survey of the relevant data in Fig. 1, which displays the  $T$  dependence of  $\sigma_1(\omega)$  below  $3000 \text{ cm}^{-1}$  for LaAlGe and CeAlGe, while its insets compare their spectra at 5 and 300 K over the entire measured spectral range. We refer to the Supplemental Material (SM) for more details on the original data [32]. Besides the  $T$ -independent absorptions at UV energy scales, which are almost identical in both compounds, we encounter a relevant  $T$  dependence in  $\sigma_1(\omega)$  from FIR up to the visible spectral range (i.e.,  $\omega < 10^4 \text{ cm}^{-1}$ ). In agreement with the  $dc$  transport results, LaAlGe and CeAlGe

are metallic, as pointed out by their Drude-like zero-energy mode which narrows with decreasing  $T$ . The  $T$  dependence at FIR and midinfrared (MIR) energies is rather distinct between the two investigated materials. In LaAlGe [Fig. 1(a)] there is a depletion of  $\sigma_1(\omega)$  below  $300 \text{ cm}^{-1}$ , signaling a spectral weight (SW) reshuffling [45] from FIR towards high frequencies, mainly up to  $1000 \text{ cm}^{-1}$ . A SW removal is also observed in the MIR energy interval (i.e.,  $1500\text{--}4000 \text{ cm}^{-1}$ ) with accompanying accumulation at even higher energies, up to the near-infrared (NIR) spectral range (i.e.,  $4000\text{--}8000 \text{ cm}^{-1}$ ). We note a qualitative similarity with the SW redistribution in the optical response of the noncentrosymmetric, transition-metal mononitride TaAs, for which type-I Weyl states as consequence of broken space-inversion symmetry [46] as well as some reminders of nodal semimetals [31] were actually envisaged. For CeAlGe [Fig. 1(b)], the SW reshuffling at FIR-MIR energy scales is less pronounced, while something equivalent to LaAlGe happens at MIR-NIR energies. Otherwise, the MIR optical conductivity is quite featureless, just displaying a moderate increase with frequency in the interval  $100\text{--}1000 \text{ cm}^{-1}$ , thus above the shallow minimum in  $\sigma_1(\omega)$  around  $100 \text{ cm}^{-1}$ , right at the onset of the Drude resonance. The trend in the charge dynamics from LaAlGe to CeAlGe is, however, different from what has been encountered in  $\text{Nd}_2(\text{Ir}_{1-x}\text{Rh}_x)_2\text{O}_7$ , for which the ground state undergoes a putative crossover from a narrow-gap Mott insulator to a Weyl semimetal and then to a correlated metal upon increasing  $x$  [47–49].

As shown in the SM [32],  $\sigma_1(\omega)$  can be well decomposed within the phenomenological Drude-Lorentz approach [30], of which we specifically highlight the reproduction of the metallic contribution [ $\sigma_1^{\text{Drude}}(\omega)$ , insets of Fig. 2]. The zero-energy mode in  $\sigma_1(\omega)$  is well accounted for by two Drude terms (Fig. S5 in the SM [32]). By subtracting those calculated Drude intraband components from the total  $\sigma_1(\omega)$  at each  $T$ , we can better emphasize its interband contribution [i.e.,  $\Delta\sigma_1(\omega) = \sigma_1(\omega) - \sigma_1^{\text{Drude}}(\omega)$ ], shown in Fig. 2 at 5 K. In both cases,  $\Delta\sigma_1(\omega)$  presents two distinct intervals (colored shaded areas in Fig. 2), characterized by (quasi) linear frequency dependencies, yet with different slopes. Even though the intervals for the linearities in  $\Delta\sigma_1(\omega)$  are rather small, the encountered behavior is definitely different from the typical optical response of type-I Weyl semimetals [31] and corresponds to the expected characteristic features describing the interband contribution in  $\sigma_1(\omega)$  for type II. Indeed, it has been theoretically shown that the tilting of the Dirac cone within a single-band framework considerably affects the overall shape of the excitation spectrum [50]. In the case of type II upon increasing the frequency, there is first a (quasilinear) sharp, steep onset of  $\Delta\sigma_1(\omega)$ , occurring at  $\omega > \Omega_1$  (turquoise area in Fig. 2), then followed by a linear frequency dependence of  $\Delta\sigma_1(\omega)$  at  $\omega > \Omega_2$  (green area in Fig. 2). The latter has a smaller slope, such that it induces a kink in  $\Delta\sigma_1(\omega)$  and it does not extrapolate to the origin in the limit  $\omega \rightarrow 0$  (red dashed line in Fig. 2), as it is instead predicted in the optical conductivity for type-I Weyl semimetals [50]. The tilting of the Weyl cones can be quantified by the tilting parameter  $\hat{w}$  (Fig. 3), which is significantly larger than one in both materials [32], thus alluding to an overtilted regime [50]. The optical response devoid of its metallic term hence allows

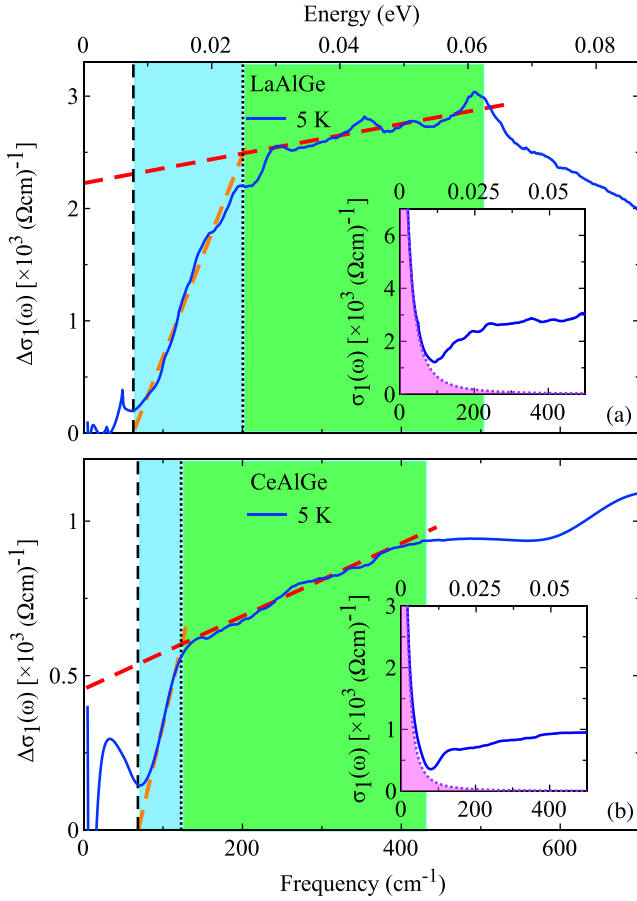


FIG. 2. Interband contribution  $\Delta\sigma_1(\omega) = \sigma_1(\omega) - \sigma_1^{\text{Drude}}(\omega)$  at 5 K for (a) LaAlGe and (b) CeAlGe, obtained by subtracting the calculated Drude intraband [ $\sigma_1^{\text{Drude}}(\omega)$ ] component from the total  $\sigma_1(\omega)$  (see insets). The thick dashed lines emphasize the linear frequency dependencies of  $\Delta\sigma_1(\omega)$ , encountered in selected energy intervals (colored shaded areas). The vertical dashed and dotted lines mark the characteristic frequencies  $\Omega_1$  and  $\Omega_2$ , respectively, which define the onset of linearities in  $\Delta\sigma_1(\omega)$  [32,50]. The insets highlight  $\sigma_1(\omega)$  at FIR energies together with the contribution  $\sigma_1^{\text{Drude}}(\omega)$  obtained within the two-Drude approach (i.e., sum of the narrow (D1) and broad (D2) Drude terms, insets of Fig. S5 in SM [32]). A similar procedure was applied at all  $T$ .

the most direct evidence of type-II Weyl semimetals and is pertinent when confirming the predictions of devoted band structure calculations, signaling the presence of so-called tilted ( $W_2$ ) Weyl cones located at  $E_F$  in both materials [21]. This is in contrast to previous attempts on  $\text{WTe}_2$  [51–53], whose Weyl states are, however, well above  $E_F$  and  $\sigma_1(\omega)$  is dominated by the (Drude) intraband component. Furthermore, since here the trivial bands are quite negligible at  $E_F$  (besides some small pockets in LaAlGe) and interband transitions involving them prosper above  $1000 \text{ cm}^{-1}$  [21], our data even overrule possible ambiguities in the interpretation of the kink in  $\Delta\sigma_1(\omega)$ , driven by the tilting of the Weyl cones, which could arise when several trivial bands close to  $E_F$  interplay with the nontrivial ones, like in Te [54].

The slope of  $\sigma_1(\omega)$  at  $\omega > \Omega_2$  turns out to be inversely proportional to  $v_F$ . We use the formalism of Ref. [50] to infer

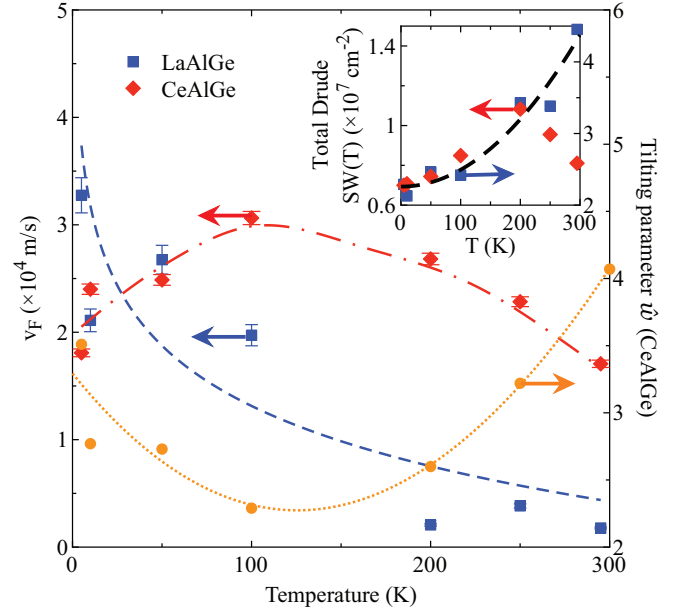


FIG. 3.  $T$  dependence of the Fermi velocity  $v_F$ , extracted from  $\Delta\sigma_1(\omega)$  (Fig. 2). The dash-dot line for CeAlGe is a guide to the eyes, while the dashed one for LaAlGe corresponds to the functional  $v_F \sim A + B \ln(1/T)$  (see text) [55]. The tilting parameter (i.e.,  $\hat{w}$  in Eq. (S3) and in Table I in SM [32]) is shown for CeAlGe as well [50]. Inset:  $T$  dependence of the total Drude SW (i.e.,  $\omega_p^2 = \omega_{p,D1}^2 + \omega_{p,D2}^2$ ,  $\omega_{p,Di}$  being the plasma frequencies of D1 and D2 Drude terms [32]), which follows a  $T^2$  behavior (thick dashed line) below 200 K for both compounds [56,57].

$v_F$  (for details we refer to the SM [32]), which is shown in Fig. 3 as a function of  $T$ . We obtain an overall increase of  $v_F$  with decreasing  $T$  in LaAlGe, while for CeAlGe  $v_F$  displays a broad maximum upon approaching 100 K, below which it evidently decreases. The low  $T$  values of  $v_F$  in LaAlGe, despite lacking momentum resolution, are very much compatible on the average with the estimation from the angle-resolved-photoemission-spectroscopy (ARPES) spectra [58] and are typical for weakly interacting Weyl semimetals [59,60]. The  $T$  dependence of  $v_F$  in LaAlGe quite agrees with the expectations for a two- and three-dimensional Dirac material within the Hartree-Fock approximation for which a  $\ln(1/T)$  behavior has been foreseen (dashed line in Fig. 3) [55]. Such a logarithmic divergence is supposed to vanish if correlation effects are taken into account [61]. We propose that the decreasing  $v_F$  below  $\sim 100$  K in CeAlGe (Fig. 3) hints at the progressive onset of correlation effects, similar to observations in  $\text{YbPtBi}$  [20] as well as in nodal-line Dirac semimetals [62]. Therefore, the broad maximum in  $v_F(T)$  of CeAlGe at 100 K (Fig. 3), coincident with the prominent change of slope in the  $dc$  transport properties (Fig. S3 in the SM [32]) at the same  $T$ , may define the  $T$  scale for the onset of correlation effects [6,12,63,64]. A similar and possibly correlations-related nonmonotonic  $T$  dependence is encountered in  $\hat{w}$  of CeAlGe (Fig. 3), as well [32]. Although the role of correlation effects is not yet fully disentangled in the Weyl semimetal  $\text{YbMnBi}_2$  [65,66] and the linear frequency dependencies of its optical conductivity look different than in

the title compounds, it is worth pointing out that its  $v_F$  is also suppressed with decreasing  $T$  [65].

So far, we centered our discussion around the interband contribution to the optical response (Figs. 2 and 3). To further elaborate on the impact of correlation effects, we now approach the intraband part of  $\sigma_1(\omega)$ . It is a generic property of correlated materials to display a strongly reduced Drude SW with respect to the (noninteracting) band theory calculations [67,68]. Moreover, theoretical calculations suggest that in Dirac and Weyl semimetals there is a SW transfer from the Drude to the interband component of  $\sigma_1(\omega)$  upon lowering  $T$  and the Drude SW itself undergoes a  $T^2$  dependence [56,57]. Such a Drude SW suppression at low  $T$  fairly applies to our findings below 200 K in both compounds (inset of Fig. 3 and SM [32]) and is also in agreement with experimental observations in other topological materials [46,48,62,69,70]. Furthermore, the coefficient of the  $T^2$  dependence of the Drude SW is inversely proportional to  $v_F$  [56,57], thus allowing its average estimation from the intraband contribution to  $\sigma_1(\omega)$  and a comparison with the  $v_F$  interband values (Fig. 3). For CeAlGe, the resulting intraband  $v_F \sim 8.1 \times 10^4$  m/s is considerably larger than the interband one at any  $T$  (Fig. 3). A discrepancy in the estimation of  $v_F$  from both the intra and interband contribution to the optical conductivity was likewise encountered in the correlated Nd<sub>2</sub>Ir<sub>2</sub>O<sub>7</sub> semimetal [48]. This may indicate that correlation effects, related to heavy Bloch states at low  $T$  (see below), are not properly considered in the approach of Refs. [56] and [57] for the  $T$  dependence of the Drude SW and caution is needed when extracting sensitive quantities from it. On the contrary, the intraband  $v_F \sim 5 \times 10^4$  m/s for LaAlGe rather agrees with its estimation at low  $T$  from  $\Delta\sigma_1(\omega)$  (Fig. 3) since correlation effects are indeed not supposed to be relevant. For the sake of completeness, it is worth mentioning that recent measurements of the  $T$ - and angular-dependent de Haas-van Alphen oscillations in LaAlGe [71] nevertheless imply very small cyclotron masses, very high  $v_F$  (up to two orders of magnitude than the low  $T$  values in Fig. 3) and consequently strongly reduced electronic specific heat, which is not compatible with the measured quantity [71,72]. This, however, signals that not all portions of the Fermi surface detected by quantum oscillations do contribute to the thermodynamic properties, which we address next in connection with the optical data.

The specific heat [ $C(T)$ ] measurements as a function of  $T$  and magnetic field in CeAlGe are indeed very instrumental towards elucidating the presence and role of electronic correlations, mediated by  $f$ -electrons. The  $C(T)$  data at zero and low fields display a peak at the magnetic transition at about 5 K, which is progressively washed out and then transformed into a broad (Schottky-type) feature upon increasing the magnetic field [26,72]. Such a behavior is reminiscent of the expectations for the screened Kondo model including antiferromagnetic interactions [73] as well as for the Kondo resonance model [74]. Here, we emphasize though the analogy with similar data in YbPtBi [20] in the spirit of a Weyl-Kondo scenario [13]. In fact, for a Weyl-Kondo semimetal the linear dispersion relation at the Weyl nodes dictates the low  $T$  dependence of  $C(T) \sim k_B(\frac{k_B T}{\hbar v_F})^3$  [13]. In

CeAlGe,  $v_F$  from  $C(T)$  at all fields [26,72] are significantly reduced (i.e.,  $v_F \sim 6-9 \times 10^3$  m/s), compared to values for LaAlGe, in a quite similar manner as in YbPtBi with respect to its reference compound LuPtBi [20]. Furthermore,  $v_F$  in CeAlGe from  $C(T)$  at zero field is roughly a factor of 3 smaller than  $v_F$  at low  $T$  inferred from  $\Delta\sigma_1(\omega)$  (Fig. 3), thus establishing a fair agreement among different experiments.

We now turn our attention to the estimation of  $m^*/m_e$ , which may be achieved from the charge dynamics in conjunction with the additional constraint given by the Sommerfeld  $\gamma$  value of the electronic component in  $C(T)$ . From its definition together with the Drude plasma frequency  $\omega_p$  it follows that  $\frac{m^*}{m_e} = (\frac{\gamma}{V_m})^{3/4} \frac{1}{\sqrt{\omega_p}}$  [12,32,75], with  $V_m$  being the molar volume [76]. We consider the total Drude SW from our phenomenological fit (inset of Fig. 3) to define the effective, total plasma frequency  $\omega_p$  [32]. With  $\gamma \simeq 1.61$  and 50 mJ/(mol K<sup>2</sup>) [71,72] we achieve  $\frac{m^*}{m_e} \simeq 2.7$  and 49 at 5 K for LaAlGe and CeAlGe, respectively. Even though the values of  $v_F$  from  $\Delta\sigma_1(\omega)$  (Fig. 3) indicate a renormalization factor of about 2, the resulting enhancement factor from  $m^*/m_e$  is approximately 20 at low  $T$  between CeAlGe and LaAlGe, with LaAlGe supplying the bare band values. It is worth underscoring that the enhancement of the optical  $m^*/m_e$  pairs with the narrowing of the metallic component in  $\sigma_1(\omega)$  of CeAlGe (i.e., reduction of the Drude scattering rates, Fig. S6 in the SM [32]). This bears testimony to a substantial band renormalization driven by Kondo-like electronic correlations [6,12].

In a broader perspective, we may then claim that the  $f$ -electrons play here different roles since they are undoubtedly involved in shaping the complex magnetism in CeAlGe [21,24–28] and equally govern the transport and thermodynamic properties, thus the physics at low-energy scales close to  $E_F$ . Our bulk sensitive optical results complement and in this specific case even outreach the (surface sensitive) ARPES experiments, which did fail, so far, in resolving the heavy Weyl fermion states.

In conclusion, upon comparing the charge dynamics of the  $f$ -electron CeAlGe with that of its reference, empty  $f$ -states LaAlGe material we provide evidence that correlation-driven Kondo physics (i.e., band-hybridization with  $f$ -electrons) affects the dispersion in momentum space near the type-II Weyl points in CeAlGe upon decreasing  $T$  below 100 K. The resulting band renormalization greatly reduces  $v_F$  and enhances the charge carriers  $m^*/m_e$  in CeAlGe with respect to LaAlGe, both revealing a heavy Weyl-Kondo state [13]. How precisely the present results and drawn conclusions might be influenced by the controversial magnetic transition [24–28] in CeAlGe at low  $T$  remains to be determined by future studies. Furthermore, Berry curvature fields associated with the Weyl nodes at  $E_F$  generate an intrinsic (topological) anomalous Hall effect, which should survive and get enhanced at low  $T$  into the correlated state, as evinced in YbPtBi [20] and Ce<sub>3</sub>Bi<sub>4</sub>Pd<sub>3</sub> [19]. In this context, the ferromagnetic PrAlGe Weyl semimetal [21], characterized by a large anomalous Hall effect [77,78], sparks our interest in chasing the related spectroscopic signatures [64]; the ongoing investigations



of its charge dynamics will be of relevance as a proof of concept.

Work at Brookhaven National Laboratory was supported by the U.S. Department of Energy, Office of Basic Energy Science, Division of Materials Science and Engineering,

under Contract No. DE-SC0012704 (materials synthesis). This research used the 28-ID-1 beamline of the National Synchrotron Light Source II, a U.S. DOE Office of Science User Facility operated for the DOE Office of Science by Brookhaven National Laboratory under Contract No. DE-SC0012704.

- [1] M. Z. Hasan and C. L. Kane, *Rev. Mod. Phys.* **82**, 3045 (2010).
- [2] Y. Tokura, M. Kawasaki, and N. Nagaosa, *Nat. Phys.* **13**, 1056 (2017).
- [3] N. P. Armitage, E. J. Mele, and A. Vishwanath, *Rev. Mod. Phys.* **90**, 015001 (2018).
- [4] H. Weyl, *Z. Phys.* **56**, 330 (1929).
- [5] A. A. Burkov, M. D. Hook, and L. Balents, *Phys. Rev. B* **84**, 235126 (2011).
- [6] D. N. Basov, R. D. Averitt, D. van der Marel, M. Dressel, and K. Haule, *Rev. Mod. Phys.* **83**, 471 (2011).
- [7] Y. Li and F. D. M. Haldane, *Phys. Rev. Lett.* **120**, 067003 (2018).
- [8] E. Bobrow, C. Sun, and Y. Li, *Phys. Rev. Research* **2**, 012078(R) (2020).
- [9] Z. Wang and S.-C. Zhang, *Phys. Rev. B* **87**, 161107(R) (2013).
- [10] W. Shi, B. J. Wieder, H. L. Meyerheim, Y. Sun, Y. Zhang, Y. Li, L. Shen, Y. Qi, L. Yang, J. Jena, P. Werner, K. Koepf, S. Parkin, Y. Chen, C. Felser, B. A. Bernevig, and Z. Wang, *Nat. Phys.* **17**, 381 (2021).
- [11] T. Morimoto and N. Nagaosa, *Sci. Rep.* **6**, 19853 (2016).
- [12] L. Degiorgi, *Rev. Mod. Phys.* **71**, 687 (1999), and references therein.
- [13] H.-H. Lai, S. E. Grefe, S. Paschen, and Q. Si, *Proc. Natl. Acad. Sci. USA* **115**, 93 (2018).
- [14] P.-Y. Chang and P. Coleman, *Phys. Rev. B* **97**, 155134 (2018).
- [15] H.-R. Chang, J. Zhou, S.-X. Wang, W.-Y. Shan, and D. Xiao, *Phys. Rev. B* **92**, 241103(R) (2015).
- [16] A. K. Mitchell and L. Fritz, *Phys. Rev. B* **92**, 121109(R) (2015).
- [17] Y. Xu, C. Yue, H. Weng, and X. Dai, *Phys. Rev. X* **7**, 011027 (2017).
- [18] S. Dzsaber, L. Prochaska, A. Sidorenko, G. Eguchi, R. Svagera, M. Waas, A. Prokofiev, Q. Si, and S. Paschen, *Phys. Rev. Lett.* **118**, 246601 (2017).
- [19] S. Dzsaber, X. Yan, M. Taupin, G. Eguchi, A. Prokofiev, T. Shiroka, P. Blaha, O. Rubel, S. E. Grefe, H.-H. Lai, Q. Si, and S. Paschen, *Proc. Natl. Acad. Sci. USA* **118**, e2013386118 (2021).
- [20] C. Y. Guo, F. Wu, Z. Z. Wu, M. Smidman, C. Cao, A. Bostwick, C. Jozwiak, E. Rotenberg, Y. Liu, F. Steglich, and H. Q. Yuan, *Nat. Commun.* **9**, 4622 (2018).
- [21] G. Chang, B. Singh, S.-Y. Xu, G. Bian, S.-M. Huang, C.-H. Hsu, I. Belopolski, N. Alidoust, D. S. Sanchez, H. Zheng, H. Lu, X. Zhang, Y. Bian, T.-R. Chang, H.-T. Jeng, A. Bansil, H. Hsu, S. Jia, T. Neupert, H. Lin *et al.*, *Phys. Rev. B* **97**, 041104(R) (2018).
- [22] Y. Xu, F. Zhang, and C. Zhang, *Phys. Rev. Lett.* **115**, 265304 (2015).
- [23] A. A. Soluyanov, D. Gresch, Z. Wang, Q. Wu, M. Troyer, X. Dai, and B. A. Bernevig, *Nature (London)* **527**, 495 (2015).
- [24] S. Dhar, S. Patalwar, and R. Vijayaraghavan, *J. Magn. Magn. Mater.* **104-107**, 1303 (1992), proceedings of the International Conference on Magnetism, Part II.
- [25] P. Puphal, C. Mielke, N. Kumar, Y. Soh, T. Shang, M. Medarde, J. S. White, and E. Pomjakushina, *Phys. Rev. Materials* **3**, 024204 (2019).
- [26] K. Singh and K. Mukherjee, *Philos. Mag.* **100**, 1771 (2020).
- [27] P. Puphal, V. Pomjakushina, N. Kanazawa, V. Ukleev, D. J. Gawryluk, J. Ma, M. Naamneh, N. C. Plumb, L. Keller, R. Cubitt, E. Pomjakushina, and J. S. White, *Phys. Rev. Lett.* **124**, 017202 (2020).
- [28] H. Hodovanets, C. J. Eckberg, Y. Eo, D. J. Campbell, P. Y. Zavaliy, P. Piccoli, T. Metz, H. Kim, J. S. Higgins, and J. Paglione, [arXiv:2101.10411](https://arxiv.org/abs/2101.10411).
- [29] J. Wang, B. Lian, and S.-C. Zhang, *SPIN* **09**, 1940013 (2019).
- [30] M. Dressel and G. Gruner, *Electrodynamics of Solids* (Cambridge University Press, Cambridge, England, 2002).
- [31] A. V. Pronin and M. Dressel, *Phys. Status Solidi B* **258**, 2000027 (2021), and references therein.
- [32] See Supplemental Material at <http://link.aps.org/supplemental/10.1103/PhysRevB.104.L121112> for additional information on the samples growth and properties, experimental techniques, and data analysis, which includes the additional Refs. [33–44].
- [33] E. Gladyshevskii, N. Nakonechna, K. Cenozal, R. Gladyshevskii, and J.-L. Jorda, *J. Alloys Compd.* **296**, 265 (2000).
- [34] J. Kieffer, V. Valls, N. Blanc, and C. Hennig, *J. Synchrotron Radiat.* **27**, 558 (2020).
- [35] B. H. Toby and R. B. Von Dreele, *J. Appl. Crystallogr.* **46**, 544 (2013).
- [36] P. Puphal, S. Kriebber, E. Suard, R. Cubitt, C. Wang, T. Shang, V. Ukleev, J. S. White, and E. Pomjakushina, *Phys. Rev. B* **101**, 214416 (2020).
- [37] Y. M. Dai, A. Akrap, S. L. Bud'ko, P. C. Canfield, and C. C. Homes, *Phys. Rev. B* **94**, 195142 (2016).
- [38] L. Z. Maulana, Z. Li, E. Uykur, K. Manna, S. Polatkan, C. Felser, M. Dressel, and A. V. Pronin, *Phys. Rev. B* **103**, 115206 (2021).
- [39] S. M. Mekonen, C.-J. Kang, D. Chaudhuri, D. Barbalas, S. Ran, G. Kotliar, N. P. Butch, and N. P. Armitage, [arXiv:2105.05121](https://arxiv.org/abs/2105.05121).
- [40] M. F. Hundley, J. D. Thompson, P. C. Canfield, and Z. Fisk, *Phys. Rev. B* **56**, 8098 (1997).
- [41] D. Tay, T. Shang, P. Puphal, E. Pomjakushina, H.-R. Ott, and T. Shiroka, *Phys. Rev. B* **102**, 241109(R) (2020).
- [42] P. Hosur, S. A. Parameswaran, and A. Vishwanath, *Phys. Rev. Lett.* **108**, 046602 (2012).
- [43] L. Benfatto and E. Cappelluti, *Phys. Rev. B* **78**, 115434 (2008).
- [44] B. Xu, L. X. Zhao, P. Marsik, E. Sheveleva, F. Lyzwa, Y. M. Dai, G. F. Chen, X. G. Qiu, and C. Bernhard, *Phys. Rev. Lett.* **121**, 187401 (2018).

- [45] The spectral weight ( $SW$ ) of the optical conductivity corresponds to its integral  $SW(T) = \frac{Z_0}{\pi^2} \int_{\omega_1}^{\omega_2} \sigma_1(\omega'; T) d\omega'$ , expressed in units of  $\text{cm}^{-2}$  ( $Z_0 = 376.73 \Omega$ , being the impedance of free space) [30].  $\omega_i$  ( $i = 1$  and  $2$ ) define the energy interval, relevant for the  $SW$  estimation.
- [46] B. Xu, Y. M. Dai, L. X. Zhao, K. Wang, R. Yang, W. Zhang, J. Y. Liu, H. Xiao, G. F. Chen, A. J. Taylor, D. A. Yarotski, R. P. Prasankumar, and X. G. Qiu, *Phys. Rev. B* **93**, 121110(R) (2016).
- [47] K. Ueda, J. Fujioka, Y. Takahashi, T. Suzuki, S. Ishiwata, Y. Taguchi, and Y. Tokura, *Phys. Rev. Lett.* **109**, 136402 (2012).
- [48] K. Wang, B. Xu, C. W. Rischau, N. Bachar, B. Michon, J. Teyssier, Y. Qiu, T. Ohtsuki, B. Cheng, N. P. Armitage, S. Nakatsuji, and D. van der Marel, *Nat. Phys.* **16**, 1194 (2020).
- [49] Even though the optical data of  $\text{Nd}_2\text{Ir}_2\text{O}_7$  are rather similar in both Refs. [47,48], it is fair to mention the discrepancy concerning its ground state, proposed to be paramagnetic in a single-crystal [48] and antiferromagnetic in a polycrystalline [47] sample.
- [50] J. P. Carbotte, *Phys. Rev. B* **94**, 165111 (2016).
- [51] C. C. Homes, M. N. Ali, and R. J. Cava, *Phys. Rev. B* **92**, 161109(R) (2015).
- [52] A. J. Frenzel, C. C. Homes, Q. D. Gibson, Y. M. Shao, K. W. Post, A. Charnukha, R. J. Cava, and D. N. Basov, *Phys. Rev. B* **95**, 245140 (2017).
- [53] S.-i. Kimura, Y. Nakajima, Z. Mita, R. Jha, R. Higashinaka, T. D. Matsuda, and Y. Aoki, *Phys. Rev. B* **99**, 195203 (2019).
- [54] D. Rodriguez, A. A. Tsirlin, T. Biesner, T. Ueno, T. Takahashi, K. Kobayashi, M. Dressel, and E. Uykur, *Phys. Rev. Lett.* **124**, 136402 (2020).
- [55] F. Setiawan and S. Das Sarma, *Phys. Rev. B* **92**, 235103 (2015).
- [56] P. E. C. Ashby and J. P. Carbotte, *Phys. Rev. B* **89**, 245121 (2014).
- [57] C. J. Tabert, J. P. Carbotte, and E. J. Nicol, *Phys. Rev. B* **93**, 085426 (2016).
- [58] S.-Y. Xu, N. Alidoust, G. Chang, H. Lu, B. Singh, I. Belopolski, D. S. Sanchez, X. Zhang, G. Bian, H. Zheng, M.-A. Husanu, Y. Bian, S.-M. Huang, C.-H. Hsu, T.-R. Chang, H.-T. Jeng, A. Bansil, T. Neupert, V. N. Strocov, H. Lin *et al.*, *Sci. Adv.* **3**, 6 (2017).
- [59] S.-Y. Xu, I. Belopolski, D. S. Sanchez, C. Zhang, G. Chang, C. Guo, G. Bian, Z. Yuan, H. Lu, T.-R. Chang, P. P. Shibayev, M. L. Prokopovych, N. Alidoust, H. Zheng, C.-C. Lee, S.-M. Huang, R. Sankar, F. Chou, C.-H. Hsu, H.-T. Jeng *et al.*, *Sci. Adv.* **1**, 10 (2015).
- [60] B. Q. Lv, H. M. Weng, B. B. Fu, X. P. Wang, H. Miao, J. Ma, P. Richard, X. C. Huang, L. X. Zhao, G. F. Chen, Z. Fang, X. Dai, T. Qian, and H. Ding, *Phys. Rev. X* **5**, 031013 (2015).
- [61] S. Das Sarma, E. H. Hwang, and W.-K. Tse, *Phys. Rev. B* **75**, 121406(R) (2007).
- [62] Y. Shao, A. N. Rudenko, J. Hu, Z. Sun, Y. Zhu, S. Moon, A. J. Millis, S. Yuan, A. I. Lichtenstein, D. Smirnov, Z. Q. Mao, M. I. Katsnelson, and D. N. Basov, *Nat. Phys.* **16**, 636 (2020).
- [63] Y. Zhang, H. Lu, X. Zhu, S. Tan, W. Feng, Q. Liu, W. Zhang, Q. Chen, Y. Liu, X. Luo, D. Xie, L. Luo, Z. Zhang, and X. Lai, *Sci. Adv.* **4**, 1 (2018).
- [64] M. Corasaniti, R. Yang, K. Sen, K. Willa, M. Merz, A. A. Haghighirad, M. Le Tacon, and L. Degiorgi, *Phys. Rev. B* **102**, 161109(R) (2020).
- [65] M. Chinotti, A. Pal, W. J. Ren, C. Petrovic, and L. Degiorgi, *Phys. Rev. B* **94**, 245101 (2016).
- [66] D. Chaudhuri, B. Cheng, A. Yaresko, Q. D. Gibson, R. J. Cava, and N. P. Armitage, *Phys. Rev. B* **96**, 075151 (2017).
- [67] M. M. Qazilbash, J. J. Hamlin, R. E. Baumbach, L. Zhang, D. J. Singh, M. B. Maple, and D. N. Basov, *Nat. Phys.* **5**, 647 (2009).
- [68] L. Degiorgi, *New J. Phys.* **13**, 023011 (2011).
- [69] B. Xu, Z. Fang, M.-Á. Sánchez-Martínez, J. W. F. Venderbos, Z. Ni, T. Qiu, K. Manna, K. Wang, J. Paglione, C. Bernhard, C. Felser, E. J. Mele, A. G. Grushin, A. M. Rappe, and L. Wu, *Proc. Natl. Acad. Sci. USA* **117**, 27104 (2020).
- [70] R. Yang, T. Zhang, L. Zhou, Y. Dai, Z. Liao, H. Weng, and X. Qiu, *Phys. Rev. Lett.* **124**, 077403 (2020).
- [71] Z. Hu, Q. Du, Y. Liu, D. Graf, and C. Petrovic, *Appl. Phys. Lett.* **117**, 222410 (2020).
- [72] H. Hodovanets, C. J. Eckberg, P. Y. Zavalij, H. Kim, W.-C. Lin, M. Zic, D. J. Campbell, J. S. Higgins, and J. Paglione, *Phys. Rev. B* **98**, 245132 (2018).
- [73] J. Rech, P. Coleman, G. Zarand, and O. Parcollet, *Phys. Rev. Lett.* **96**, 016601 (2006).
- [74] K. Schotte and U. Schotte, *Phys. Lett. A* **55**, 38 (1975).
- [75] N. W. Ashcroft and N. D. Mermin, *Solid State Physics* (Holt-Saunders, Philadelphia, 1976).
- [76] The molar volumes are  $41.92 \times 10^{-6}$  and  $40.89 \times 10^{-6}$   $\text{m}^3/\text{mole}$  for  $\text{LaAlGe}$  and  $\text{CeAlGe}$ , respectively: [https://materials.springer.com/isp/crystallographic/docs/sd\\_1406403](https://materials.springer.com/isp/crystallographic/docs/sd_1406403) and Ref. [72].
- [77] B. Meng, H. Wu, Y. Qiu, C. Wang, Y. Liu, Z. Xia, S. Yuan, H. Chang, and Z. Tian, *APL Mater.* **7**, 051110 (2019).
- [78] D. S. Sanchez, G. Chang, I. Belopolski, H. Lu, J.-X. Yin, N. Alidoust, X. Xu, T. A. Cochran, X. Zhang, Y. Bian, S. S. Zhang, Y.-Y. Liu, J. Ma, G. Bian, H. Lin, S.-Y. Xu, S. Jia, and M. Z. Hasan, *Nat. Commun.* **11**, 3356 (2020).